A clean, robust 3D medial axis

Bastien Durix, Kathryn Leonard, Sylvie Chambon, Géraldine Morin

A clean, robust 3D medial axis

Durix Bastien[1], Leonard Kathryn[2], Morin Géraldine[1], Chambon Sylvie[1]

bastien.durix@irit.fr, kleonard.ci@gmail.com, geraldine.morin@irit.fr, sylvie.chambon@irit.fr
[1] IRIT
[2] Occidental College

Abstract

Computing the medial axis of a 3D surface mesh is challenging. Points on the discrete medial axis can be defined as interior Voronoï vertices of the surface mesh, but the resulting medial structure rarely has clean connectivity and consistent geometry. In this paper, we provide a medial axis computation based on the Voronoï diagram able to generate manifold medial sheets with coherent topology and geometry, generating consistent geometric structures similar to those in the continuous setting. Because of the correspondences between the surface mesh and resulting medial mesh, we also provide an efficient way to separate the shape into coherent regions associated to medial structures. This correspondence allows for a medial-axis-based filtration of surface structures to generate a Hausdorff ε-approximation of the surface points based on a simplified medial axis, thereby providing a robust medial representation with guaranteed surface approximation.

Keywords: Skeleton, structure, mesh, delaunay, voronoï

1. Introduction

Medial representations are quite popular in computer graphics because they combine implicit and explicit shape representations, and offer a lower dimensional model of a 3D shape, the skeleton, that captures the geometric information from the boundary, while a radius or distance function describes the interior of the shape. The first such model, the Blum medial axis, was introduced in [Blu73] for 2D shapes. It consists of a skeleton and a radius function defined at each point of the skeleton that gives the distance of the skeleton point to the boundary. A useful discretization of the Blum medial axis relies on a shape's Delaunay triangulation and its dual, the Voronoi diagram.

As described in [TDS*16], several approaches exist to compute a full skeleton. Voxel-based methods [HR08, ADBS11] which are a 3D version of classical 2D thinning methods, easily maintain the structure of the shape, and can be less subject to noise. In [JST15], the voxel grid is the support of a mass transport process, leading to a multiscale, simplified skeleton. In [YLJ18], the authors use a Delaunay tetrahedralization of the open voxels of a shape boundary to compute a voxel core that converges to the true medial axis as the voxelization of the shape becomes dense. A separate pruning step then removes noisy elements in the voxel core with a guarantee on the approximation and the homotopy equivalence. In these approaches, the shape must first be converted to a voxel grid, and its sampling density is directly linked to the skeleton accuracy, thereby introducing an additional parameter to the model. Also, in the voxel based approaches, no global and topologically coherent structure of the skeleton is available. Other methods compute a skeleton from boundary samples [RAV*19, MBC12, LBKP21]. Each boundary sample is characterized by a position and a normal, and no additional structure is needed. A set of tangent spheres can then be computed, filtering any non-descriptive ones. Methods based on deep learning have also been proposed. In [YYW*20], a simplified skeleton is computed and accurately describes the shape (depending on the chosen precision) but they do not capture the shape structure, as the resulting skeleton is typically not a graph. In [CD23] the local structure of the skeleton is preserved in general, but there is no guarantee on the coherence of the connectivity, that is, a tetrahedron may belong to the resulting skeleton. In fact, by construction ~~Most explicit~~ deep learning methods do not maintain a clear relationship to the shape boundary. In [RLS*21], the shape and its skeleton are linked but the representation is implicit, giving neither connectivity nor structure.

Other approaches, including ours, are based on the computation of a Voronoi diagram. For simple shapes such as polyhedra, the Voronoi diagram can be explicitly computed [SPB96]. The power crust applies a power diagram to compute a mesh and a skeleton from a disorganized point cloud [ACK01].

Underlying many of these methods is an attempt to address the major drawback of the medial axis in applications: a lack of stability, in that a small change on the shape boundary can produce large changes in the medial axis. Moreover, edges linked to several medial axis surface sheet may appear in non singular regions, leading to connectivity and structural inconsistencies. Many approaches have been proposed to construct a robust medial axis for 3D shapes, with varying degrees of success. Classical approaches to robustness

are based on pruning [DZ03, AL01] prune the Voronoi diagram to obtain a sensible medial structure. [YSC*16] compute a significance measure: the authors demonstrate that a global measure related to Erosion Thickness, generalized from 2D to 3D, is more efficient than a local measure. The well-known Scale Axis Transform [MGP10] has the advantage of taking into account multiple medial representations. They propose a multi-scale representation through the scale axis transform that takes into account a scaling of medial balls, but the approach results in some artifacts that require a separate pruning step. This method has generated multiple variants and improvements [LWS*15, PWG*19] that produce a simplification of a Voronoi skeleton. However, these methods do not maintain a robust link to the 3D mesh. In contrast, our goal in the current work is to be independent of a pruning step. We both maintain global connectivity consistency in the structure of the medial axis and geometric consistency with the surface mesh, in the sense that the Delaunay tetradhedralization of the output surface mesh is dual to the output Voronoi skeleton.

Many researchers compute a curve skeleton, which is a network of curves, instead of the full skeleton in 3D, [CSM07, SYJT13]. A curve skeleton is appealing because it addresses the previously mentioned instability while capturing most of the major structures of the shape. It can be estimated by mesh contraction [ATC*08, LW18, ZLZ20], or through the computation of a 3D skeleton [DS06, TAOZ12], or directly from the mesh, using tools such as local separators [BR21]. Curve skeletons necessarily maintain only a weak relationship to the surface mesh, however, and there are some shape structures (funnel shapes, for example) that are not well-suited for description by a single curve.

Depending on particular goals and applications for a skeletal model, different properties of the skeleton may be desired, such as continuity, connectivity, geometric correspondence with the boundary, or a particular level of simplicity. These variations in goals have produced variations in skeletonization algorithms that make different trade-offs, as the work cited in the previous paragraphs demonstrates. In this article, we take as input a Delaunay surface mesh of a shape and compute a medial axis that has a full array of desirable properties. This approach is similar to a 2D skeletonization method by propagation [DCL*19, DMC*19], where the skeleton is computed step by step, and where a Hausdorff distance criterion identifies noise so that insignificant parts of the medial axis are not computed. The next section describes this simplified skeletonization.

1.1. Simplified skeletonization

In this paper, we present a method to compute a simplified, robust medial axis for a 3D shape from a Delaunay input mesh representing the shape surface. Our approach is based on a propagation of medial balls, or equivalently, Delaunay tetrahedra, which means we do not require a pruning step. A Delaunay tetrahedron is a tetrahedron such that its circumscribed sphere does not contain any other point from the surface mesh. Therefore, each skeletal point is associated to a tetrahedron, and the edges between skeletal points are associated to tetrahedra that share faces. Finally, a Delaunay mesh is a mesh for which each triangle is a triangle from a Delaunay tetrahedron. Local geometry is combined into a global structure on the skeleton, which is then used for the simplification analysis. This global structure consists of sheets, which are surface portions of the skeleton, boundary paths, which are curve boundaries of a single sheet, and singular paths, which are curve portions separating different sheets (See Section 3 for details). As a result, our approach guarantees the following properties (*cf.* Figure 1):

- **The topological and geometric relationships between the surface and medial meshes are preserved.** Specifically, (a) the resulting medial mesh is homotopically equivalent to the output surface mesh by construction, and (b) the points on the medial mesh are Voronoi duals of Delaunay tetrahedra generated by the surface mesh. Each vertex, edge, face and sheet of the medial axis corresponds to a well-specified set of vertices, edges, faces, or region of the surface mesh. This means that we maintain correspondence between the surface and medial meshes.
- **The geometric structures of the medial mesh are clean and coherent.** The skeleton is divided into sub-structures of sheets with topologically consistent manifold interiors, which are separated and bounded by manifold paths. The skeleton mesh itself is connected for an input shape with a single component due to the homotopy equivalence.
- **The simplified medial axis provides a guaranteed ε-approximation to the original surface points.** The simplified medial mesh generated for some choice of $\varepsilon > 0$ corresponds to a subset of the original surface points that are ε-close in Hausdorff distance to the original surface points. All topological features at a scale larger than ε are maintained, though features at a scale smaller than ε may be deleted.

In what follows, we first describe the continuous and discrete constructions of the interior Blum medial axis (BMA) in Section 2. In Section 3, we describe the global structures of the discrete BMA and describe how these are related to local structures. Finally, we describe the algorithm for generating the simplified skeleton based on the ε error parameter in Section 4, and present results in Section 5. We also include a brief appendix to explain some special cases that arise in this discrete setting, and how we handle them.

2. Geometry of the interior medial axis

The Blum medial axis is structured into parts that offers strong geometric properties in the smooth setting; we seek and provide analogs in the discrete setting. In this section, we describe these properties and the correspondences between smooth and discrete representations.

2.1. Smooth setting

In this section, we recall the structure of the medial axis in the smooth setting where the shape surface is differentiable, in order to provide an analogy with the discrete setting we are interested in.

Given a closed, non-self-intersecting surface $S \subset \mathbb{R}^3$ with continuous curvature and a finite set of curvature extrema and ridge curves, the interior Blum medial axis can be defined as the locus of centers of maximally inscribed spheres within the surface, together with their radii. This produces a skeleton composed of sphere centers that is a Whitney stratified set M with a finite number of strata.

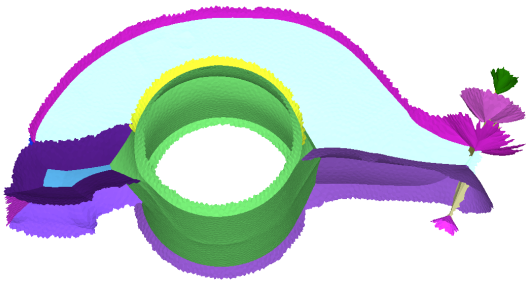

(a) Subdivision of a skeleton into sheets

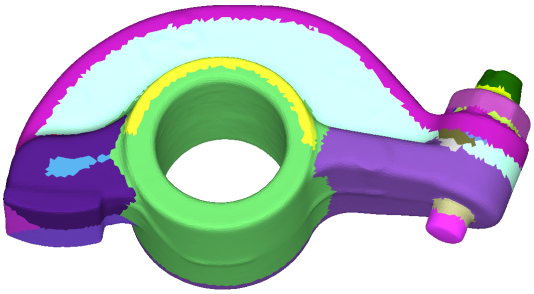

(b) Surface mesh regions associated to each sheet of the skeleton

Figure 1: Global structures of the skeleton (a), and their consistency with the surface mesh (b). The color coding in the figures shows which global skeletal structures in (a) correspond to which global shape structures in (b).

The points of M are traced out by the centers of the inscribing spheres resulting in a medial skeleton composed of smooth surfaces and curves joined along well-understood singularities. A radius function r is defined for each point of M, giving the associated radius of the inscribing sphere. Intuitively, a Whitney stratified set is an arrangement of nicely behaved sets called strata, so that any non-empty intersection of strata is a manifold of lower dimension, the intersection is transverse, and the tangent spaces of the strata converge appropriately at these intersections. See, for example, [Dam05] for details.

In the case of the medial axis for the surface of a 3D shape, such as in Figure 2, each stratum is either a 2D medial sheet (in light blue in the figure), a 1D medial curve (in red – generically, these will be 2D), an intersection point or curve where two higher dimensional strata meet (in black), or a boundary point or curve bounding a higher dimensional stratum (in blue). See [GK04] for an exhaustive classification of medial axis points. Away from singularities and sheet or curve boundaries, the degree of differentiability of M is equal to the degree of differentiability of S.

As a stratified set, the points of M are generically one of three types, see Figure 2:

1. **Regular points** in the interior of a top-dimensional stratum, in light blue. For regular points, the medial spheres are bitangent to S, which means that each point of M corresponds to two points of S, one on either side of M (“above" and “below").

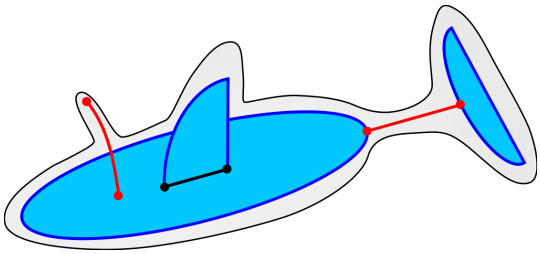

Figure 2: A skeleton structure in the continuous setting: a continuous shape and its skeleton containing three medial sheets (and corresponding strata). Regular skeleton points (in light blue) lie in the interior of a skeleton sheet. They are bounded by singular boundary points (in blue), and intersect at interior singular curves (in black). The medial axis also contains two non-generic medial strata of lower dimension, curves (in red).

2. **Singular interior** points where two strata intersect, in black. For singular interior points, the medial spheres will be at least tri-tangent to S, corresponding to the merging of bitangencies on at least two strata meeting along the singularity.
3. **Singular boundary points** where the inscribing sphere osculates at an extremum of at least one principal curvature, in blue. For singular boundary points, the medial sphere has only one tangency, the point of extremal curvature, corresponding to the merging of at least one bitangency where the points “above" and “below" merge into a single point.

2.2. Discrete setting

A primary contribution of our paper is to construct well-defined discrete versions of the medial structures described for differentiable shape surfaces in the previous section. In applications, the smooth surface S described above is typically replaced by a sampling of its points and connectivity between those points, a surface mesh consisting of vertices joined by edges and faces. Similarly, the smooth strata of the medial skeleton are replaced by a medial mesh. In what follows, we assume sampled points of a 3D shape surface are vertices in a Delaunay surface mesh S, with an induced medial mesh M. Points on M can then be computed as interior Voronoi vertices generated by the surface points. Because the Voronoi vertices will be centers of the circumspheres of its dual, the Delaunay tetrahedralization of the volume enclosed by S, the tetrahedra will provide a discrete analogue of medial balls in the smooth case. Similarly, distance from the Voronoi vertices to the surface points will provide a discrete version of the radius function r. As the sampling on the surface becomes dense, converging to the smooth surface, a subset of this discrete medial skeleton converges to the smooth skeleton [DZ03].

With this characterization, much of the structure from the differentiable setting carries over. The resulting discrete M will have three types of points, see Figure 3 for illustration:

1. **Regular points**, in (3a). For regular points, each point of M will typically correspond to a tetrahedron that crosses the interior of S, with three points of S on one side of M and one point on the other side (“above" and “below"), see left, but other

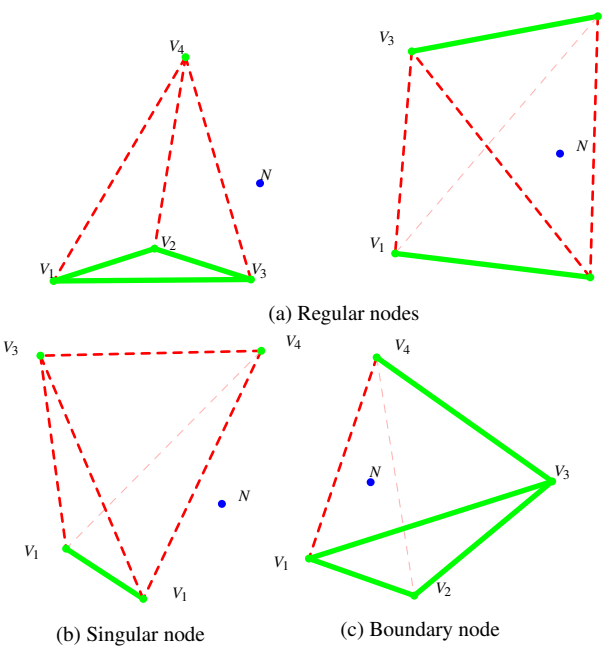

(a) Regular nodes

(b) Singular node

(c) Boundary node

Figure 3: A sampling of some different (non-exhaustive) configurations for a discrete medial node N, in blue, corresponding to different point type classifications of N. The vertices $(V_i)_{i=1...4}$ are its corresponding boundary points and tetrahedron. Among the tetrahedral edges, the green edges belong to the surface mesh and the red dashed ones traverse the volume inside the 3D shape. Note that the node N is not necessarily inside the tetrahedron.

configurations are possible such as two points above and two below [CDE*00], see right.

2. **Singular interior points**, in (3b). For singular interior points, the tetrahedron will correspond to the convergence of tetrahedra of regular points on at least two strata meeting along the singularity. In this case, there will be at least two sets of points above and below corresponding to at least three disconnected regions of the surface.
3. **Singular boundary points**, but without a notion of tangency, in (3c). For singular boundary points, the points in S composing the tetrahedron will be adjacent and belong to a single connected component, with the two “sides" of M having converged.

This framework gives the foundation for the structures we use to generate the strata of the discrete skeleton. Unfortunately, guarantees of topological and geometric coherence from the smooth setting do not automatically carry over, as rounding errors and other issues often lead to medial skeletons with more complicated structures [TDS*16]. Our algorithm addresses these issues to produce a geometrically coherent skeleton.

3. Hierarchical structure of the discrete skeleton

In what follows, we distinguish between local medial structures (e.g., medial points and neighbors, corresponding surface points and neighbors) and global medial structures (e.g., medial sheets, boundaries, singular sets). Our algorithm analyzes local structures to build coherent global structures.

The constructions presented in this section are necessary for understanding the algorithm in Section 4. We define the global medial structures in Section 3.5, which allow us to segment the surface correspondingly in Section 3.2. In section 3.3, we present the local medial structures, derived from the Voronoi and Delaunay duality linking the surface mesh to the medial mesh, that provide the basis for the global structures and also for the simplification of the medial skeleton. Section 3.4 describes how the global structures are obtained from the local structures. Finally, section 3.5 describes how we compute the simplified 3D medial axis.

3.1. Global structures of the discrete skeleton

Medial sheets are typically two-dimensional for a 3D shape, but can also be one-dimensional. Sheet boundaries and singular paths are typically one-dimensional, but can also be zero-dimensional. For simplicity, we present our algorithm for two-dimensional case, but the process is analogous in the one-dimensional or zero-dimensional cases.

Sheets, the top-dimensional strata described in Section 2, are the fundamental building blocks of the skeleton. We define a discrete *sheet* of the medial axis to be a connected set of regular medial points for which the corresponding regions on the surface mesh have two connected components, together with any neighboring singular points (corresponding to more than two connected components) or boundary points (corresponding to one connected component) (see Figure 3). Each sheet corresponds to one or more connected portions of the input surface mesh. Furthermore, each sheet has two sides, and can be therefore viewed as two *oriented sheets*, where each oriented sheet corresponds to a different side of the surface mesh, “above" or “below", see Figures 4a and 4b).

The non-regular medial points associated to a sheet are members of either a *boundary path*, Figure 4c, corresponding to the ridge curves on the shape surface where the two sides of the surface correspondence of a medial sheet have merged, or a *singular path*, Figure 4d, where two medial sheets intersect, or both. The boundary and singular paths are typically 1D strata. Boundary paths with no singular points belong to a single sheet, but all singular paths belong to multiple sheets. When boundary points are also singular, it is because a singular set has intersected a boundary path.

These global medial structures correspond to structures on the surface mesh S. Sheets correspond to coherent regions of the shape surface, such as protrusions. Boundary paths correspond to curvature extrema in the surface, such as ridges. Singular paths correspond to closed paths on the surface delineating connections between coherent shape regions. Finally, we note that a path within a sheet, which means a path of regular points, generates two paths on the shape surface: one “above" and one “below". This means that each surface path can be attributed to one of the two oriented sheets associated to a medial sheet.

3.2. Segmenting the surface using sheets and paths

Using these global structures, we can segment the shape surface into coherent regions. In Figure 4, we associate the singular path

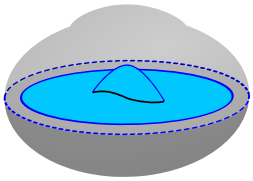

(a) Mesh portion covered by the lower main sheet in darker gray

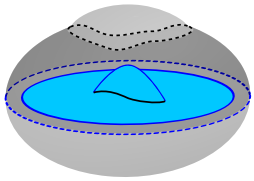

(b) Mesh portion covered by the upper main sheet in dark gray

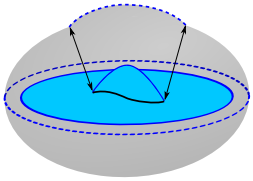

(c) Boundary paths are dashed

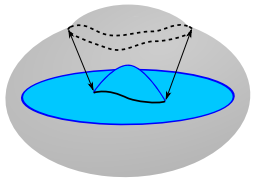

(d) Singular path is dashed

Figure 4: Correspondences between skeletal structures and surface regions. Solid line boundary paths (darker blue) and singular paths (black) represent paths on the mesh. Dashed paths represent the corresponding paths on the surface mesh. (a) The medial boundary path of the main (horizontal) sheet separates the surface into two regions, above and below, with the lower region shown in darker gray. (b) The upper surface region, however, is interrupted by region associated to the smaller medial sheet that is connected to one side of the main sheet. The singular path separating the two sheets corresponds to the black dashed path on the surface mesh and the resulting dark gray region corresponds to the surface that is above the main sheet. (c) If a medial boundary path is not a closed loop, the surface path will also not be a loop, as can be seen in the surface path generated by the medial boundary of the smaller sheet. If a medial boundary path is a loop, the corresponding path on the surface mesh will also be a loop, as can be seen in the surface path generated by boundary of the main medial sheet. (d) For medial singular paths, in contrast, a medial path that is an interval can correspond to a surface path that is a loop, as can be seen in the path on the surface mesh that corresponds to the closed black medial singular path.

separating two sheets to a closed path on the shape surface that delineates the coherent surface region associated to that sheet. In Figure 4, consider the upper part of the object where there is a small medial sheet connected to the larger one. The small sheet corresponds to a small portion of the surface of the object that is surrounded by the dashed black loop induced by the black singular path at the base of the medial sheet. Repeating this analysis for each sheet in a medial axis produces a segmentation of the shape boundary where shape segments are bounded by surface loops induced by singular paths in the medial axis. This will be important in Section 4 where we determine whether or not to compute a sheet in the medial axis by evaluating the contribution of the corresponding shape segment to the overall shape.

3.3. Local structures of the discrete skeleton

The global structures described in the previous section can be formed by aggregation of the appropriate local structures. Philosophically, the aggregation is straightforward – join connected sets of points that are regular, or singular, or boundary – but many local degeneracies arise in practice (some of which are collected in Appendix A) that make the process challenging. We now define the local structures that will allow us to generate global structures.

3.3.1. Voronoi and Delaunay duality between the skeleton and the surface mesh

Based on a Delaunay triangulation of a surface mesh S, we construct the Delaunay tetrahedralization T of the volume of the interior of S. T is the dual of the Voronoi diagram V of the vertices of S. Each of S, M, T, and V have vertices, edges, and faces, and T also has tetrahedra.

All vertices of T are vertices of the surface mesh. Note that while all edges and faces of S belong to the Delaunay tetrahedralization T, only a subset of edges and faces of T belong to S. Because of the number of types of collections of vertices, edges, and faces, we specify vocabulary and color-code mesh elements consistently in the text and figures to distinguish between them. All vertices, edges, faces (triangles in the general setting), and volumes (tetrahedra in the general setting) belonging to the Delaunay tetrahedralization are colored in red. We identify the edges and faces that cross the volume of the interior of S by appending the word *volumetric*. The faces of the Delaunay tetrahedralization that are also faces of the surface S are colored in green and carry the word *surface*.

Similarly for V, almost all vertices interior to S belong to the medial mesh M [DZ03], while only a subset of the edges and faces of V are contained in M. The elements in the Voronoi diagram V are colored in dark blue except for the subset of the elements that belong to the medial axis M, which are lighter blue. We refer to the faces of V as *Voronoi faces* to emphasize that they are not typically triangular. Identifying the faces, edges, and vertices of V that are completely inside the volume bounded by S defines the interior discrete medial axis that is our primary object of study. Note that there are also Voronoi vertices, edges, and faces that are completely outside the volume bounded by S. These define an exterior medial skeleton that we do not study here.

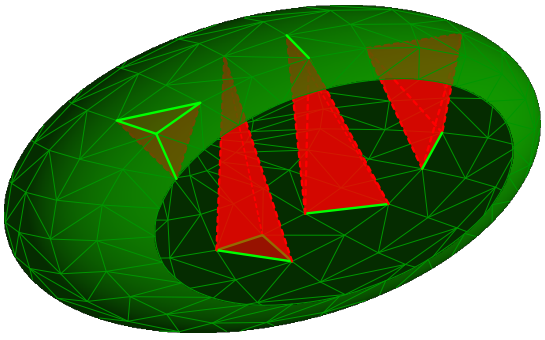

Figure 5: Difference between volumetric and surface tetrahedral components. Surface edges and faces (green) lie on the mesh of the object, while volumetric edges and faces (red) cross the volume of the object. The shapes of the drawn tetrahedra refer to Figure 3.

We illustrate the local constructions more precisely next, emphasizing the duality between them: the Delaunay tetrahedralization

T, which is primal, creates connectivity between surface vertices through the shape interior. In the typical case, this generates:

- edges, joining two surface points, that may be a surface edge (Figures 5 and 3, plain green edges), or volumetric edges (Figures 5 and 3, dashed red edges);
- triangles, joining three surface points, that may be a surface triangle in which case, its three edges are also surface edges (Figures 5 and 3, green triangles), or a volumetric triangle (Figures 5 and 3, red triangles);
- tetrahedron, joining four surface points that are volumetric, since we consider only the interior Delaunay tetrahedra (Figures 5, red tetrahedra).

These primal elements have corresponding dual elements in V :

- tetrahedra correspond to Voronoi vertices which are centers of the circumspheres of the tetrahedra;
- tetrahedral faces correspond to Voronoi edges;
- tetrahedral edges correspond to Voronoi faces. Note that a *medial face*, and more generally a Voronoi face, is a planar polygon since it lies on the medial plane of the dual edge and can have an arbitrary number of nodes.

- medial vertices are a subset of Voronoi vertices and we denote them as *nodes*;
- medial edges are a subset of Voronoi edges;
- medial faces are a subset of Voronoi faces.

We construct our simplified medial axis by exploring the Voronoi diagram to determine which elements to include in the medial axis, and then computing the medial axis components according to their importance to the overall shape as measured by the Hausdorff distance between the original corresponding surface points and the simplified version. The process requires both local and global considerations of both primal and dual components.

Around a given medial edge, there can be as many Voronoi faces as there are Delaunay edges (including volumetric edges and surface edges) around the associated Delaunay face. This means that edges are not necessarily surrounded by 3 Voronoi faces. A Voronoi face dual to a Delaunay edge that belongs to the surface, that is, dual to a surface edge, is called an *open Voronoi face*, *cf.* Figure 6. An open Voronoi face contains a node that is outside the shape boundary. This type of Voronoi face does not belong to the skeleton of the medial axis, because it is not entirely contained in the interior S. This allows us to filter out Voronoi face that are not part of the interior medial axis.

Using the same idea, an *open edge* is associated to a Delaunay face that belongs to the surface mesh. For this type of edge, one of its extremities is a Voronoi nodes on the inner medial axis, and the other one is a Voronoi vertex on the outer medial axis. Like the open Voronoi face, the open edge therefore crosses the surface S. Naturally, an open Voronoi face contains at least one open edge. These edges do not belong to the medial mesh.

3.3.2. Oriented medial edges and faces

As discussed in Section 3.2, medial sheets comprising the skeleton have two sides; each side corresponds to a region of the shape surface that is either “above" or “below." This two-sidedness also applies to our local structures, producing two-sided edges and two-sided face that we denote by half edges and half facets, as in [DRJ15]. As shown in Figure 7, on a degree 3 edge, three face are connected, which gives six half facet. In total, six half edges are derived from a degree 3 edge, one for each half facet. For example, viewing a singular path as composed of a succession of half edges will result in a path that lies on a single side of a sheet.

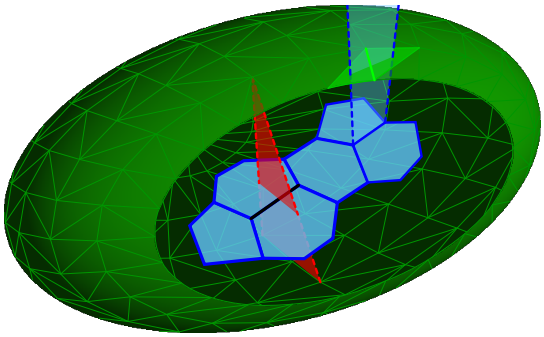

Figure 6: Illustration of the relationship between skeleton and surface components. An open skeletal edge (dashed blue) is associated to its dual, a surface mesh face (green triangle). An open face, containing open edges is associated to its dual, a surface mesh edge (green). This kind of face contains edges that lie on both the internal and the external skeletons. A Delaunay triangle (red) is associated to its dual, a skeletal edge (black), and each of its crossing edges (dashed red) is associated to its dual, a skeletal face.

We distinguish between the edges that are above and those below by defining two half edges for each edge in the medial mesh. These half edges will have orientations, moving in sequential order around an medial face. The half edges are in counter-clockwise order around the medial face, with respect to its normal vector. As there are two possibilities for the normal orientation, there are two sets of half edges, which are associated to the two sides of the medial face. A half medial face consists of all the half edges that are on the same side. Using the resulting graph structure to represent the skeleton, we can easily navigate between the medial faces, edges and vertices and their corresponding surface regions from the connectivity information, and we can resolve ambiguities about neighboring medial faces, since a neighbor must be on the same side of the medial mesh.

3.4. Building global from local

We now aggregate the local structures described in Section 3.3 into the global medial structures described in 3.1. In other words, we determine medial sheets and identify which of its nodes and edges are regular, singular, or belonging to the sheet boundary.

Each **sheet** is a subset of the medial faces of the skeleton. Two medial faces are on the same sheet if there exists a path of medial faces between them such that any two successive medial faces are separated by a regular edge. Collecting all medial faces contained in the same sheet produces the mesh for that sheet.

It remains to determine the regularity or singularity of the nodes

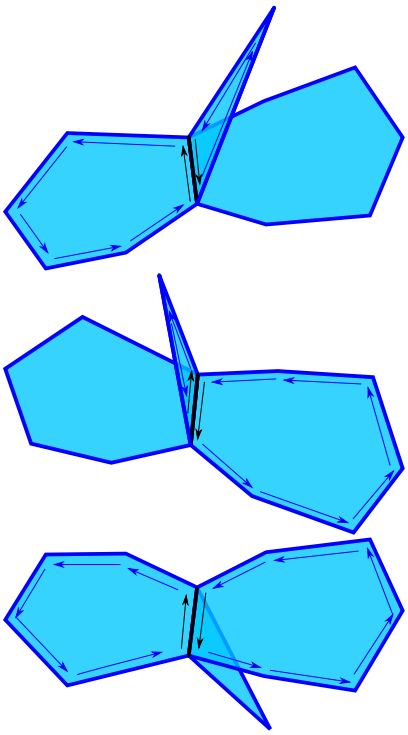

Figure 7: Representation of the half edges around a (black) singular medial edge, from different views (up left, up right, below). Around this degree 3 edge, there are 6 half edges represented by the black arrows. Each pair of (black arrows) half edges represents a different area on the surface mesh.

and edges within a (non-oriented) sheet. Recall that the degree of an edge is defined by the number of medial faces containing the edge. A singular edge is then an edge of degree 3 or more, a boundary edge is an edge of degree 1, and a regular edge is an edge of degree 2. These edges may belong to multiple sheets.

We now consider the half edges and how they compose **paths** on a sheet (*cf.* Figure 8). Since each half edge is associated to a half medial face, each of them will be associated to a unique sheet. Note that an open path of full medial edges corresponds to a closed path of half edges: one traversal of successive edges on one side of the sheet and another traversal of the same edges on the other side but with the opposite orientation. We say that two half edges are successive if they respect the following conditions:

- The last node of one half edge is the first node of the other,
- Their associated half medial faces are neighbors (or are the same).

A **half singular path**, or **singular path** (as every path in what follows will now be half edges) is defined by a set of successive half singular edges (degree 3 or more). As there are opposite half edges for each edge on an medial face, each singular path can be associated to an opposite singular path (*cf.* Figure 8).

Finally, a **boundary path** is a set of successive half boundary edges. As there are two half boundary edges for each boundary edge on an medial face, a boundary path will be traced out twice by half paths, one on each side of the sheet.

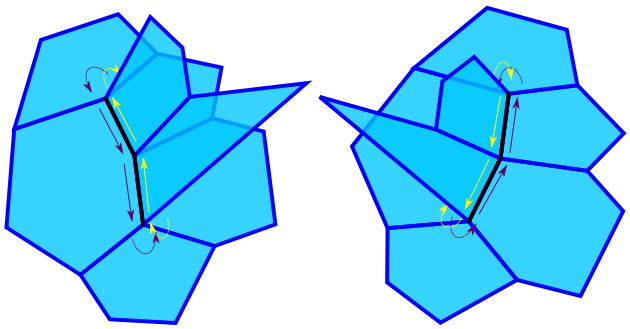

Figure 8: A path on the skeleton is a sequence of half edges. Here, we can see two sides of the same skeleton, where two paths are drawn (yellow and purple), representing the same (black) singular edges. By construction of half edges, these paths have opposite direction. Note that green and purple half paths do not lie on the same medial faces, and therefore are not on the same sheet.

In the following, we consider a specific subset of boundary and singular paths, such that all the half edges composing them are on the same sheet. In the case of the boundary path, it will help to simplify the boundary of a single sheet, and in the case of the singular path, it will separate a given sheet from other sheets.

3.4.1. Medial mesh and surface mesh correspondence

Given the global structures on the medial axis, we can recover the corresponding regions on the surface mesh (*cf.* Figure 9). Each sequence of half edges on the skeleton corresponds to a path on the surface mesh as follows: each half edge is associated to a half medial face on one side of the skeleton, and therefore determines one vertex of the surface mesh (the center of the unique Voronoi cell on which the half medial face lies). Therefore, the sequence of medial faces associated to the sequence of half edges gives us a sequence of vertices on the surface mesh. Indeed, if two medial faces are neighbors, the associated surface vertices are on the same Delaunay triangle. As they are on the same side by construction of the path, they necessarily are neighbors.

When this sequence of half edges corresponds to tracing out a half path loop along the entirety of a singular path, it generates a closed path on the surface mesh that distinguishes the surface region corresponding to the current sheet from the rest of the the shape surface.

While we primarily consider the paths on the surface mesh induced by singular skeletal paths, note that any skeletal path can be associated to a path on the surface mesh. For example, a boundary skeletal path, as it is two-sided, induces two closed paths on the surface mesh: each vertex and face between those paths is associated to a boundary skeletal node.

3.5. Evaluation of the significance of new sheets

Once a sheet has been computed, its singular edges are used to detect the singular paths that separate the current sheet from its

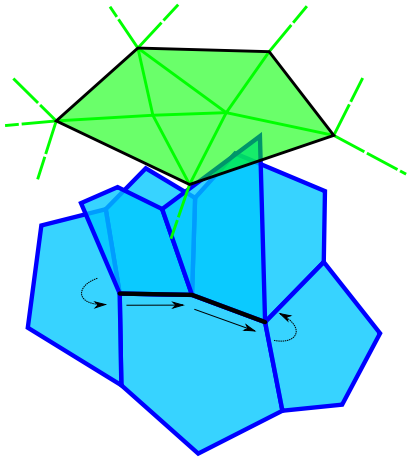

Figure 9: A (black) singular path on the skeleton associated to a (black) surface mesh path, whose vertices are the centers of the five Voronoi cells the path is crossing (as each medial face is separating two Voronoi cells). The computed surface path surrounds a surface portion for which we can evaluate an ε-significance.

neighbor sheets. Suppose we are given a tolerance parameter ε. We only wish to compute those neighbor sheets that correspond to a surface region, as described in 3.4.1, that has significance greater than ε, where significance is measured by Hausdorff distance to the original surface.

Consider a singular path contained within a computed sheet. The singular path corresponds both to a set of medial spheres centered at its nodes, and also to the corresponding surface region for the neighbor sheet whose significance we wish to determine. If the Hausdorff distance between the vertices of the surface region and the medial spheres is greater than ε, the neighbor sheet is computed. Otherwise, the sheet may be ignored: this means that the surface region is entirely covered by existing spheres of the skeleton, with a radius increased by ε (*cf.* Figure 10).

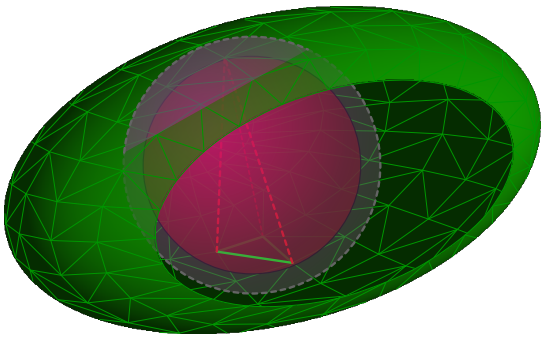

Figure 10: Illustration of the ε criterion. A tetrahedron corresponds to a unique medial ball, passing through its four vertices. Adding ε to the radius of the ball, we obtain a new (dashed) sphere, covering other vertices of the surface mesh.

4. Computing a topologically coherent and simplified skeleton representing an ε-approximation of the surface mesh

We now describe how to compute a simplified skeleton from an input surface mesh. Using the structures developed in the previous sections, we compute a provably, topologically coherent skeletal structure sheet by sheet and check if each sheet is significant for representing an ε approximation of the original shape in terms of the Hausdorff distance. As input, this method assumes a Delaunay triangular mesh (*cf.* 4.1). The pseudocode of the algorithm is given in Algorithm 1.

ALGORITHM 1: Skeletonization.

Input : $\mathcal{M}$: Delaunay mesh
Input : ε: Hausdorff distance parameter
Output: $\mathcal{S}$: Simplified skeleton
Let $\mathcal{M}_w$ be a working copy of $\mathcal{M}$
Compute Delaunay tetrahedralization of $\mathcal{M}_w$
Estimate a first medial face F of the skeleton
Compute full sheet $\mathbf{S}$ containing F
Let l_s be the list of degree 3 half edges on $\mathbf{S}$
while l_s not empty **do**
  $E = pop\_front(l_s)$
  E_{ext} = half edge neighboring E, on neighbor sheet
  P = singular path containing E_{ext}, on neighbor sheet
  C = set of faces on $\mathcal{M}_w$ covered by neighbor sheet
  d = maximal distance between skeletal spheres on P and mesh vertices on C
  if $d < \varepsilon$ **then**
    Remove faces C from $\mathcal{M}_w$
    D = set of internal Delaunay faces closing the hole
    Add faces D to $\mathcal{M}_w$
  else
    Compute neighbor sheet $\mathbf{S}_i$
    Add list of degree 3 half edges on $\mathbf{S}_i$ to l_s
  end
end
Let l_b be the list of degree 1 half edges on skeleton
while l_b not empty **do**
  E = steepest half edge of l_b
  F = set of medial faces containing E and E_n
  P = singular path separating F from the computed skeleton
  C = set of faces on $\mathcal{M}_w$ covered by the sheet beyond P
  d = distance between skeletal spheres on P and mesh vertices on C
  if $d < \varepsilon$ **then**
    Remove faces C from $\mathcal{M}_w$
    D = set of internal Delaunay faces closing the hole
    Add faces D to $\mathcal{M}_w$
end
Let l_p be the list of problematic half edges on skeleton
while l_p not empty **do**
  $E = pop\_front(l_p)$
  P = problematic path containing E
  F = set of medial faces separated by P
  Set edges of P singular
  Assign new label to faces of F
end

The algorithm proceeds through all sheets in the medial axis of the input mesh, computing those with significance above the threshold ε. We summmarize the pipeline here, then detail each step in the

paragraphs that follow. To begin, we compute a first sheet, starting from a first medial face (*cf.* 4.2) and aggregating neighboring medial faces into a complete sheet (*cf.* 4.3). Each singular medial edge is attached to a new sheet. We compute the singular path connecting this sheet (*cf.* 4.4) and determine if the significance if the sheet is greater than ε (*cf.* 3.5). If not, we discard the skeleton propagation to the insignificant sheet. If the sheet is relevant, we allow the propagation to compute the sheet. Repeating this operation over each half singular path linking a sheet will produce the full skeleton of ε-significant sheets. We then simplify the skeleton boundaries according to the same ε criterion, removing medial faces when possible (*cf.* 4.6). This step highly simplifies the resulting skeleton, removing small peaks along sheet boundaries. Finally, we ensure the sheet is manifold, removing problematic paths that create degenerate geometry (*cf.* 4.7).

4.1. Input mesh

The input of this algorithm is a Delaunay triangular mesh bounding a 3D shape. Each triangle of such a mesh is on a Delaunay tetrahedron: thus a Delaunay tetrahedron is either inside or outside the shape. As a consequence, we know which portion of the skeleton is inside, and which is outside, offering a clear labeling of outside and inside skeleton. Furthermore, because the mesh is Delaunay, a direct connection exists between the connectivity of the skeleton and the connectivity of the surface mesh, and between the topology of the skeleton and the topology of the surface mesh.

A Delaunay triangular mesh can be built from a given manifold surface mesh (*cf.* [DZM07]), using edges flipping and splitting. The vertices of the original mesh are preserved in the Delaunay mesh, and the skeletal structure we compute can still be applied to the non-Delaunay version of a mesh, though the duality will not be preserved. We also note that, since the atomic operations applied to convert a mesh into a Delaunay mesh do not affect the topology of the mesh, topology is preserved between original mesh and Delaunay mesh, and therefore maintains consistency with the skeleton.

4.2. Computing the first medial face

The algorithm starts with an initial medial face of the skeleton. We first choose a node of the skeleton. This node will likely belong to multiple medial faces, and we select one.

To compute the first node on the skeleton, we need to find an internal, or volumetric, tetrahedron. We select an arbitrary triangle of the surface mesh. As the mesh itself is a subset of the Delaunay tetrahedralization, this triangle is necessarily a face of a tetrahedron. Once this triangle is chosen, two tetrahedra are candidates to be our first tetrahedron: one interior and one exterior to the shape volume. Using the orientation of the mesh surface, we can determine which one is interior, which gives us a first interior medial node. Finally, to avoid choosing a first medial node that is not significant, we detect the neighboring node with a maximal radius (as each interior tetrahedron corresponds to a medial sphere), and iterate this operation so that that chosen initial node has a locally maximal radius.

Finally, the first medial face is randomly chosen from the medial faces surrounding the chosen node. More precisely, as an medial face is the dual of a volumetric edge, we choose one volumetric edge among the edges of the chosen interior tetrahedron which determines an medial face.

4.3. Single sheet propagation

We will assign a label to each skeletal sheet. To compute a sheet, we start from a first medial face, which we label. We then add all the neighbor medial faces sharing a regular edge in a propagation process, and assign the same label to them. We repeat the propagation for each added face, labeling the medial faces until no neighboring unlabelled medial faces sharing a regular edge remain. This process ends because the boundaries of sheets consist of singular or boundary edges which are not regular edges, and a medial sheet for a finite volume discrete surface mesh will have a finite number of medial faces.

4.4. Singular paths computation

For each half singular edge on the boundary of the processed medial sheet, a half singular edge on a neighbor sheet can be identified. From this neighbor half singular edge, a half singular path can be estimated, which is associated to the neighbor sheet. (As described in Section 3.4, a half singular path in a sheet is a set of successive half singular edges belonging to the same sheet.) Recall that a full singular path corresponds to a closed loop of half singular edges that trace out the full path twice but in opposite directions (see e.g. Figure 8).

We start from a half singular edge to form the candidate list l_s and identify a neighboring half singular edge (*cf.* Figure 11) using Algorithm 2. We iterate until the loop of half edges closes, and returns the complete singular path. We then remove every used half edge from the candidate list l_s.

ALGORITHM 2: Computing next half singular edge.

Input : Half singular edge pe
Output: Next half singular edge pe'
$pe' = pe$
do
  Find pe_f, next half edge on same medial face than pe'
  Find pe_o, opposite half edge of pe_f, on the neighbor half medial face
  Find pe', next half edge on same medial face than pe_o
while pe' is not singular;

The result of this operation is sequence of half edges, called a singular path. A given singular path can be tested to identify insignificant sheets, according to ε parameter.

4.5. Identifying an insignificant sheet beyond a singular path

If a singular path separates the current sheet from a sheet that has been determined to be insignificant according to the ε criterion, we do not compute that sheet. In order to maintain the geometric relationship between the skeleton and the mesh, we also update the connectivity of the mesh when we do not compute a sheet (*cf.* Figure 12).

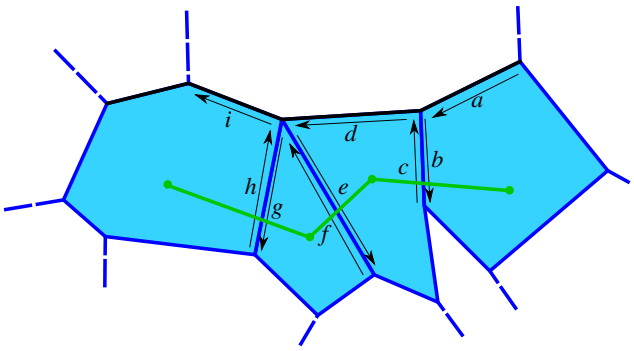

Figure 11: Identifying the next half edge to compute a singular path (here (a,d,i)). The singular edges are in black. Two examples are shown here. From a to d, we first take the next edge on the same half medial face, b, then take the opposite edge to b, c. Finally, we take the next edge to c, which is the singular edge d. More generally, to go from d to i, the same steps are repeated on each medial face until a singular half edge is found. Here, it is done twice: through half edges e, f and g, h. At this point, the singular path is composed by a, d and i. During this process, each visited half medial face belongs to a unique Voronoi cell with associated dual (green) boundary point. Each new point is stored as the next vertex of the path. When the path closes, the result is a sequence of (green) vertices creating a closed path on the boundary.

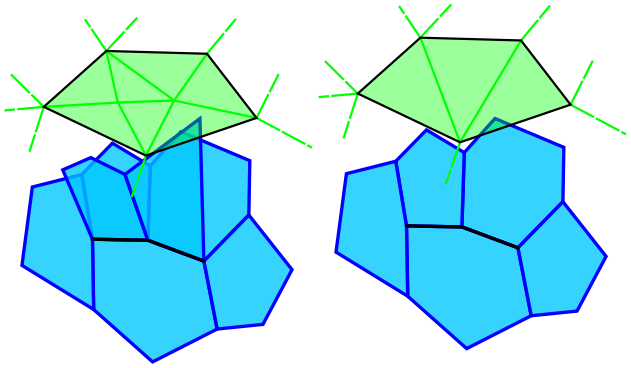

(a) Path detection

(b) Modify the mesh to ignore a sheet

Figure 12: Singular path detection and ignoring a sheet. Here, to ignore the sheet, two edges, then three faces, are created on the mesh. The mesh vertices inside the region are removed from the mesh. To ignore the sheet, the mesh vertices within the closed boundary path are removed from the mesh and the corresponding region is re-triangulated. Note that that singular edges bordering the medial path have become regular.

The main step in not computing a sheet is removing any interior tetrahedra from the object volume. This implies removing some vertices, namely vertices strictly within the region bounded by the corresponding surface path, and remeshing this portion of the surface, creating a new set of edges and faces to fill the hole.

4.6. Simplifying boundaries

Boundary paths for sheets are prone to noise. Using the same ε significance measure, we simplify sheet boundaries by removing some medial faces. We define the notion of steepness of a consecutive pair of half boundary edges to be the angle between them. At each step of the simplification (*cf.* Algorithm 1), we check the steepest consecutive half edges along the boundaries. We then compute the singular path separating those medial faces from the skeleton, and use it to check whether the sheet beyond the path can be removed using the ε criterion. If so, we remove the medial faces using same method as in 4.5.

4.7. Handling problematic paths

A computed sheet may contain some non-manifold edges. This happens when skeletal edges are connected to three medial faces that are labeled as belonging to the same sheet, violating the geometry of regular edges contained in a sheet interior. We first label these edges *problematic edges*, that is, any edge belonging to three different medial faces but labeled as members of the same sheet (see Figure 13). To resolve the problematic edges, we wish to create a new sheet, distinct from the current sheet, as shown in Figure 13. To determine the boundaries of the new sheet, we resolve a problematic path by joining problematic edges together with selected regular edges to border and be part of a new sheet's singular set. We then select the medial faces separated off by this path and create the new sheet by labeling them with a new label, as described in Algorithm 3. Splitting the new sheet from the original sheet resolves the problematic edges.

ALGORITHM 3: Correcting problematic edges.

Input : Problematic half edge *pe*
Output: Set of medial faces with new label
Output: Set of degree 2 edges set as singular
P = Path of problematic half edges containing *pe*
N = Extremity of P non connected directly to a boundary edge
S = Path of regular edges starting from N to boundary nodes of skeleton
Set S edges singular
F = Separated skeletal faces
Assign new label to faces of F

5. Results

To evaluate our methods, we apply them to 3D models from two popular databases using our implementation in Rust (`https://gitfront.io/r/user-9550748/S7fN8WFhKSkg/compact-skel-3d/`):

- The McGill database [SZM*08], which aggregates different classical databases, such as Princeton's, and the authors own models (`http://www.cim.mcgill.ca/~shape/benchMark/`).
- The Lavoué database [LCSL18](`https://perso.liris.cnrs.fr/guillaume.lavoue/data/saliency/`).

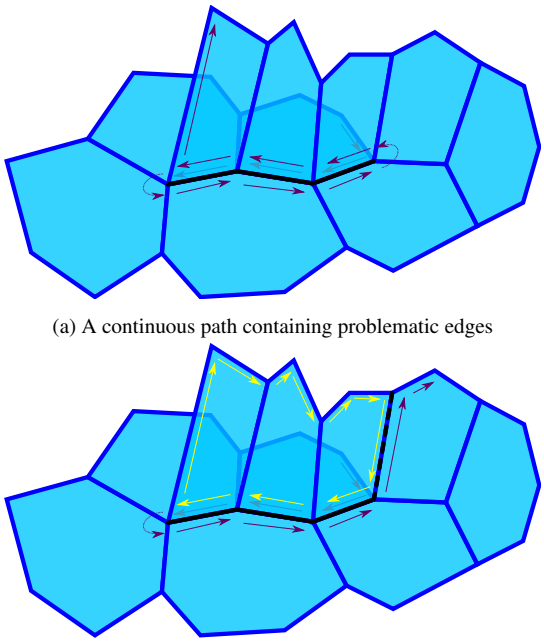

(a) A continuous path containing problematic edges

(b) Adding artificial singular edges (dashed black) separates the sheet in two parts and reformulates the problematic edges

Figure 13: An example of problematic edges, and their resolution. A problematic edge belongs to three medial faces belonging to the same sheet. Note that in (a), all medial faces belong to the same sheet even though there are some faces connected by singular edges. In (a), the black edges are problematic because they are not cleanly separating two sheets. This situation cannot be characterized locally, but requires the full computation of the sheet to detect. Our solution is to relabel appropriate regular edges as singular edges (new edge in dashed black in the bottom figure) in order to split the affected medial faces into two separate sheets. In (b), the medial faces surrounded by the yellow edges now belong to a separate sheet. This means that singular edges (black edges in the bottom figure) now belong to at most two medial faces belonging to the same sheet.

We require manifold meshes, and so all non-manifold mesh are discarded. Moreover, our algorithm assumes that we have Delaunay meshes. Some meshes of these two databases are not Delaunay, and so we apply Dyer's algorithm [DZM07] to convert them to Delaunay.

In total, we have tested our algorithm on 411 models (in supplementary material), with meshes with between 3000 and 30,000 vertices in the McGill database, and around 20,000 vertices in the Lavoué database. Skeletonization takes in average less than one minute per mesh, depending on the complexity of the given model.

Some examples are shown on Figure 14. For these examples, we set ε as 1% of the bounding box diagonal. Our algorithm can accept Delaunay meshes of arbitrary genus. As shown in Figure 14, our algorithm separates the skeleton into different sheets which are highlighted (right side of figure), and these sheets correspond to surface mesh regions (left side of figure). The structure of the skeleton is then easily accessible and usable.

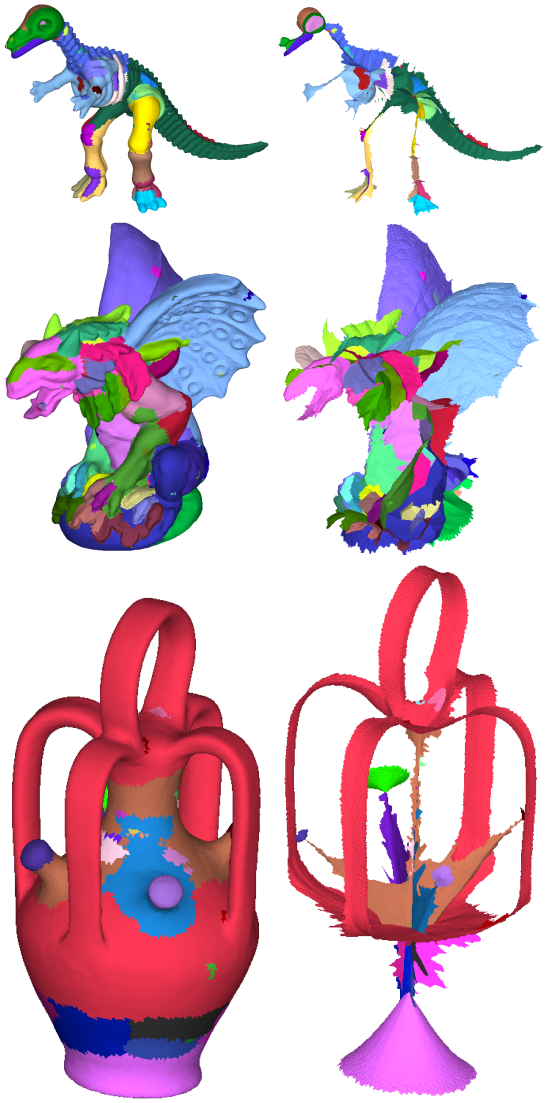

Figure 14: Skeletons computed with our algorithm, with $\varepsilon = 0.01$. To highlight the link between skeletal sheets and mesh portions, we use the same color for a skeletal sheet (right) and its associated mesh portion (left).

In Figure 18, we compare our approach to Voxel Core [YLJ18] and Scale Axis Transform (SAT) [MGP10]. Our method consistently retains salient shape features across different types of shape configurations, unlike the other two, while maintaining a similar level of cleanliness. For example, SAT erodes important regions of the body of the bunny. Similarly, Voxel Core erodes important regions of the tool (bottom left) and the head and the wings of the dragon, as well as legs of the chair. This is because our method explicitly preserves ε-fidelity with the input surface vertices while simultaneously seeking geometric coherence. In other words, we

have the additional advantage that we maintain geometric consistency with the surface mesh.

In Figure 15, we show skeletons of the same object computed with different values of ε. As ε increases from 0.00, to 0.01, and to 0.05, successive sheets are removed, but we can see a larger difference between 0.00 and 0.01 than between 0.01 and 0.05. This may suggest that each input shape has an intrinsically appropriate ε value.

Figure 16 shows skeleton computed with $\varepsilon = 0$. These skeletons have many spurious peaks.

Figure 17 shows effects of noise in the input surface mesh. We observe that even if more skeletal peaks are present on the thin parts, the global skeleton stays clean.

6. Conclusion

In this article, we present a 3D skeletonization approach to produce a simplified and geometrically consistent medial axis. Our algorithm identifies the primary structures in the medial skeleton, which are medial sheets and curves, and their boundaries, which are singular or boundary structures. These structures are topologically valid, manifold, and cleanly separated, thereby maintaining the Whitney stratified structure of the Blum medial axis in the discrete setting. Furthermore, we maintain the relationship between the surface mesh and the medial axis by associating nodes, edges, and medial faces of the skeleton with tetrahedra, triangles and edges of the Delaunay structure generated by the surface mesh points.

Using these medial structures, we compute a simplified skeleton, excluding insignificant sheets. Using the geometric links between the mesh and the skeleton, we evaluate the relevance of a skeletal sheet by evaluating the deviation from the surface mesh that would result from removing the surface region associated to that sheet. As a result, we do not compute insignificant sheets for which the Hausdorff distance of the points in the associated region of the surface mesh to the remaining surface points is lower than an ε threshold.

Future work might explore the relationship between the noise level of the surface mesh and optimal ε values for several distributions of noise. Additionally, exploring preprocessing approaches to allow for more general formats for surface data beyond Delaunay meshes would be useful.

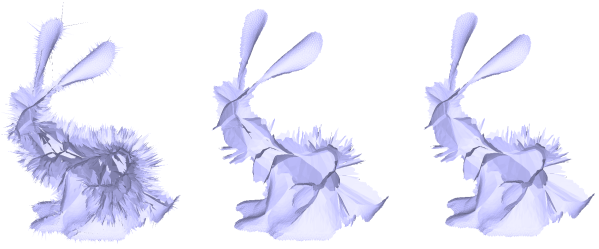

(a) $\varepsilon = 0$ (b) $\varepsilon = 0.01$ (c) $\varepsilon = 0.05$

Figure 15: Comparison of the same skeleton with different ε values. Between 15a and 15b, we can see that most of the noisy peaks were removed. Few sheets were removed between 15b and 15c.

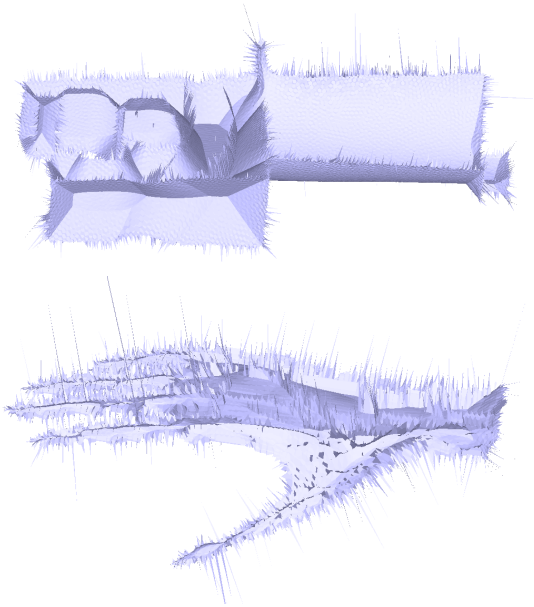

Figure 16: Computed skeleton without simplification ($\varepsilon = 0$). Unwanted peaks appear, including peaks going outside of the mesh.

Appendix A: Irregularities of the discrete skeleton

Generating the medial mesh from the Voronoi/Delaunay structures of the surface mesh, even a nice one, can produce geometric irregularities. These can be classified into two different categories: numerical problems, which come from the fact we manipulate floating point numbers instead of real numbers, and discrete skeleton problems, which are problems arising from particular configurations of the surface points, potentially breaking the properties of continuous skeletons.

- There can be more than 4 mesh points on a particular sphere, and more than 3 points on a Delaunay face. Tetrahedra and triangles are the most frequent type of Delaunay polyhedra, but not the only one. The Delaunay library we use, Tetgen [Si15] computes only standard tetrahedra, which avoids the problem, but this can result in flat (very low volume) tetrahedra.
- More than three sheets can share the same singular set, which means singular paths can lie on more than three sheets. Therefore, when separating two sheets, several half singular paths can be computed. When we test if a new sheet has to be computed, we compute the half singular path which lies on the new sheet (as explained in 4.4).
- Though it is rare, some “sheets" may be one-dimensional in certain places or in their entirety (for example, an arm that is a long circular cylinder will have a curve as its skeleton). We handle these cases separately: instead of propagating medial faces, we compute successive degree 0 edges.
- Two singular paths can cross each other: this situation is not generic behavior in the continuous setting, but can happen in the discrete setting.
- Some medial nodes can be associated to a sphere outside the mesh (*cf.* Figure 16). This is because, for some interior boundary

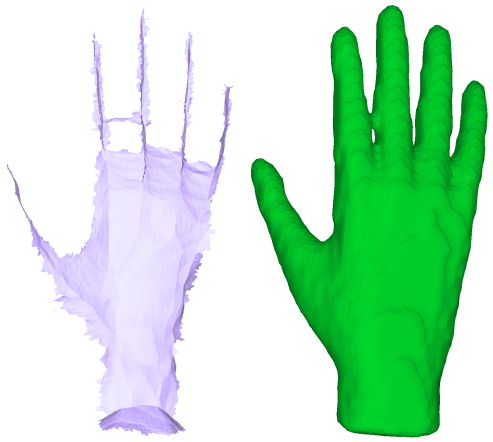

(a) Skeleton and mesh without noise

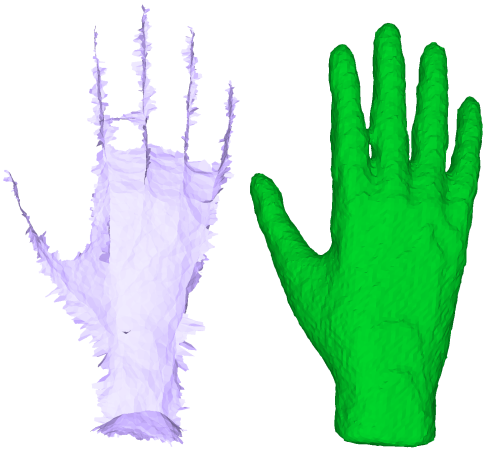

(b) Skeleton and mesh with noise

Figure 17: Effect of the mesh noise on the skeleton ($\varepsilon = 0.01$).

tetrahedra, the associated sphere center will be outside of the mesh. This can happen due to overly coarse surface sampling or to flat tetrahedra. Our algorithm detects and removes these nodes by removing the associated tetrahedra.

- As shown on Figure 13, some edges can be problematic, as they separate three medial faces from the same sheet. This problem, specific to the discrete case, is addressed in Section 4.7.

References

[ACK01] AMENTA N., CHOI S., KOLLURI R. K.: The power crust. In ACM symposium on Solid modeling and applications (May 2001), pp. 249–266. 1

[ADBS11] ARCELLI C., DI BAJA G. S., SERINO L.: Distance-driven skeletonization in voxel images. IEEE transactions on Pattern Analysis and Machine Intelligence 33, 4 (2011), 709–720. 1

[AL01] ATTALI D., LACHAUD J.-O.: Delaunay conforming iso-surface, skeleton extraction and noise removal. Computational Geometry 19, 2-3 (2001), 175–189. 2

[ATC*08] AU O. K.-C., TAI C.-L., CHU H.-K., COHEN-OR D., LEE T.-Y.: Skeleton extraction by mesh contraction. ACM Transactions on Graphics 27, 3 (2008), 1–10. 2

[Blu73] BLUM H.: Biological shape and visual science. Journal of theoretical Biology 38, 2 (1973), 205–287. 1

[BR21] BÆRENTZEN A., ROTENBERG E.: Skeletonization via local separators. ACM Transactions on Graphics 40, 5 (2021), 1–18. 2

[CD23] CLÉMOT M., DIGNE J.: Neural skeleton: Implicit neural representation away from the surface. Computers & Graphics 114 (2023), 368–378. 1

[CDE*00] CHENG S.-W., DEY T. K., EDELSBRUNNER H., FACELLO M. A., TENG S.-H.: Silver exudation. Journal of the ACM 47, 5 (Sept. 2000), 883–904. 4

[CSM07] CORNEA N. D., SILVER D., MIN P.: Curve-skeleton properties, applications, and algorithms. IEEE Transactions on visualization and computer graphics 13, 3 (2007), 530. 2

[Dam05] DAMON J.: Determining the geometry of boundaries of objects from medial data. International Journal of Computer Vision 63, 1 (June 2005), 45–64. 3

[DCL*19] DURIX B., CHAMBON S., LEONARD K., MARI J.-L., MORIN G.: The propagated skeleton: A robust detail-preserving approach. In International Conference on Discrete Geometry for Computer Imagery (2019), pp. 343–354. 2

[DMC*19] DURIX B., MORIN G., CHAMBON S., MARI J.-L., LEONARD K.: One-step compact skeletonization. In 40th Annual Conference of the European Association for Computer Graphics-Eurographics 2019 (2019), pp. 1–5. 2

[DRJ15] DYEDOV V., RAY N., JIAO X.: Ahf: array-based half-facet data structure for mixed-dimensional and non-manifold meshes. Engineering with Computers 31 (2015), 389–404. 6

[DS06] DEY T. K., SUN J.: Defining and computing curve-skeletons with medial geodesic function. In Proceedings of the Fourth Eurographics Symposium on Geometry Processing (Goslar, DEU, 2006), SGP '06, Eurographics Association, p. 143–152. 2

[DZ03] DEY T. K., ZHAO W.: Approximating the medial axis from the voronoi diagram with a convergence guarantee. Algorithmica 38, 1 (Oct. 2003), 179–200. 2, 3, 5

[DZM07] DYER R., ZHANG H., MÖLLER T.: Delaunay mesh construction. In Eurographics Symposium on Geometry Processing 2007 (July 2007). 9, 11

[GK04] GIBLIN P., KIMIA B. B.: A formal classification of 3d medial axis points and their local geometry. IEEE transactions on Pattern Analysis and Machine Intelligence 26, 2 (2004), 238–251. 3

[HR08] HESSELINK W. H., ROERDINK J. B.: Euclidean skeletons of digital image and volume data in linear time by the integer medial axis transform. IEEE transactions on Pattern Analysis and Machine Intelligence 30, 12 (2008), 2204–2217. 1

[JST15] JALBA A. C., SOBIECKI A., TELEA A. C.: An unified multiscale framework for planar, surface, and curve skeletonization. IEEE transactions on pattern analysis and machine intelligence 38, 1 (2015), 30–45. 1

[LBKP21] LEE Y., BAEK J., KIM Y. M., PARK F. C.: Imat: The iterative medial axis transform. In Computer Graphics Forum (2021), vol. 40, Wiley Online Library, pp. 162–181. 1

[LCSL18] LAVOUÉ G., CORDIER F., SEO H., LARABI M.-C.: Visual attention for rendered 3d shapes. In Computer Graphics Forum (Eurographics) (2018), vol. 37, pp. 191–203. 10

[LW18] LI L., WANG W.: Improved use of lop for curve skeleton extraction. In Computer Graphics Forum (2018), vol. 37, pp. 313–323. 2

[LWS*15] LI P., WANG B., SUN F., GUO X., ZHANG C., WANG W.: Q-mat: Computing medial axis transform by quadratic error minimization. ACM Transactions on Graphics 35, 1 (2015), 1–16. 2

[MBC12] MA J., BAE S. W., CHOI S.: 3d medial axis point approximation using nearest neighbors and the normal field. The Visual Computer 28, 1 (2012), 7–19. 1

[MGP10] MIKLOS B., GIESEN J., PAULY M.: Discrete Scale Axis Representations for 3D Geometry. In ACM Special Interest Group on Computer Graphics and Interactive Techniques Conference, SIGGRAPH (2010), vol. 29, pp. 1–10. 2, 11

[PWG*19] PAN Y., WANG B., GUO X., ZENG H., MA Y., WANG W.: Q-mat+: An error-controllable and feature-sensitive simplification algorithm for medial axis transform. Computer Aided Geometric Design 71 (2019), 16–29. 2

[RAV*19] REBAIN D., ANGLES B., VALENTIN J., VINING N., PEETHAMBARAN J., IZADI S., TAGLIASACCHI A.: Lsmat least squares medial axis transform. In Computer Graphics Forum (2019), vol. 38, pp. 5–18. 1

[RLS*21] REBAIN D., LI K., SITZMANN V., YAZDANI S., YI K. M., TAGLIASACCHI A.: Deep medial fields. arXiv preprint arXiv:2106.03804 (2021). 1

[Si15] SI H.: Tetgen, a delaunay-based quality tetrahedral mesh generator. ACM Transactions on Mathematical Software 41, 2 (2015). 12

[SPB96] SHERBROOKE E. C., PATRIKALAKIS N. M., BRISSON E.: An algorithm for the medial axis transform of 3d polyhedral solids. IEEE transactions on visualization and computer graphics 2, 1 (1996), 44–61. 1

[SYJT13] SOBIECKI A., YASAN H. C., JALBA A. C., TELEA A. C.: Qualitative comparison of contraction-based curve skeletonization methods. In International Symposium on Mathematical Morphology and Its Applications to Signal and Image Processing (2013), pp. 425–439. 2

[SZM*08] SIDDIQI K., ZHANG J., MACRINI D., SHOKOUFANDEH A., BOUIX S., DICKINSON S.: Retrieving articulated 3d models using medial surfaces. Machine Vision Application 19, 4 (2008), 261–274. 10

[TAOZ12] TAGLIASACCHI A., ALHASHIM I., OLSON M., ZHANG H.: Mean curvature skeletons. In Computer Graphics Forum (2012), vol. 31, pp. 1735–1744. 2

[TDS*16] TAGLIASACCHI A., DELAME T., SPAGNUOLO M., AMENTA N., TELEA A.: 3D skeletons: A state-of-the-art report. In Computer Graphics Forum (Eurographics) (2016), vol. 35, pp. 573–597. 1, 4

[YLJ18] YAN Y., LETSCHER D., JU T.: Voxel cores: Efficient, robust, and provably good approximation of 3d medial axes. ACM Transactions on Graphics 37, 4 (2018), 1–13. 1, 11

[YSC*16] YAN Y., SYKES K., CHAMBERS E., LETSCHER D., JU T.: Erosion thickness on medial axes of 3d shapes. ACM Transactions on Graphics 35, 1 (July 2016), 1–12. 2

[YYW*20] YANG B., YAO J., WANG B., HU J., PAN Y., PAN T., WANG W., GUO X.: P2mat-net: Learning medial axis transform from sparse point clouds. Computer Aided Geometric Design 80 (2020), 101874. 1

[ZLZ20] ZHOU J., LIU J., ZHANG M.: Curve skeleton extraction via k-nearest-neighbors based contraction. International Journal of Applied Mathematics and Computer Science 30, 1 (2020). 2

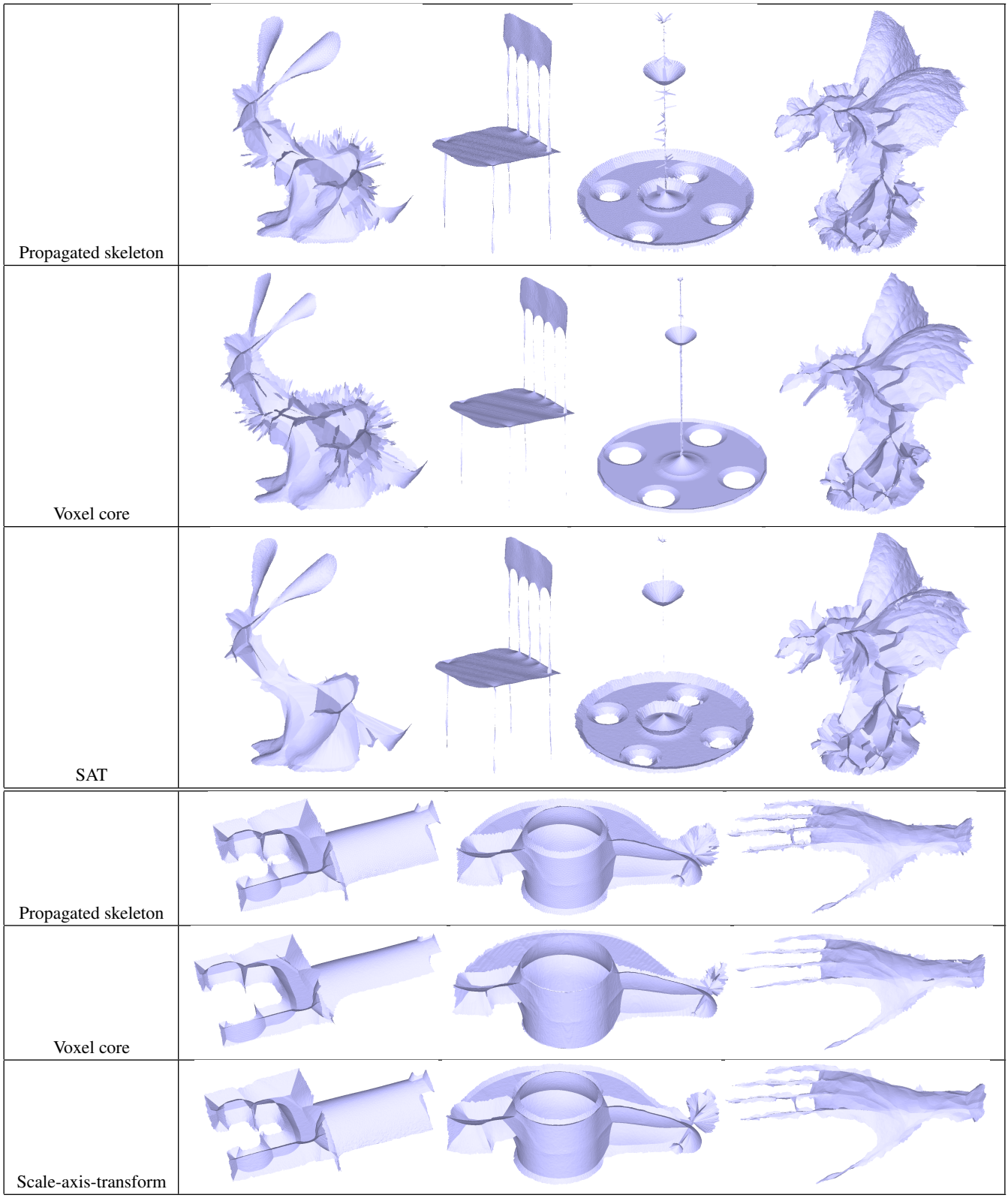

Figure 18: Comparison between our approach ($\varepsilon = 0.01$), voxelcore ($\lambda = 0.04$) and scale-axis-transform ($s = 1.1$). Because of the resolution of the image it seems that the skeleton disconnects but the topology of the skeleton is kept in all approaches.

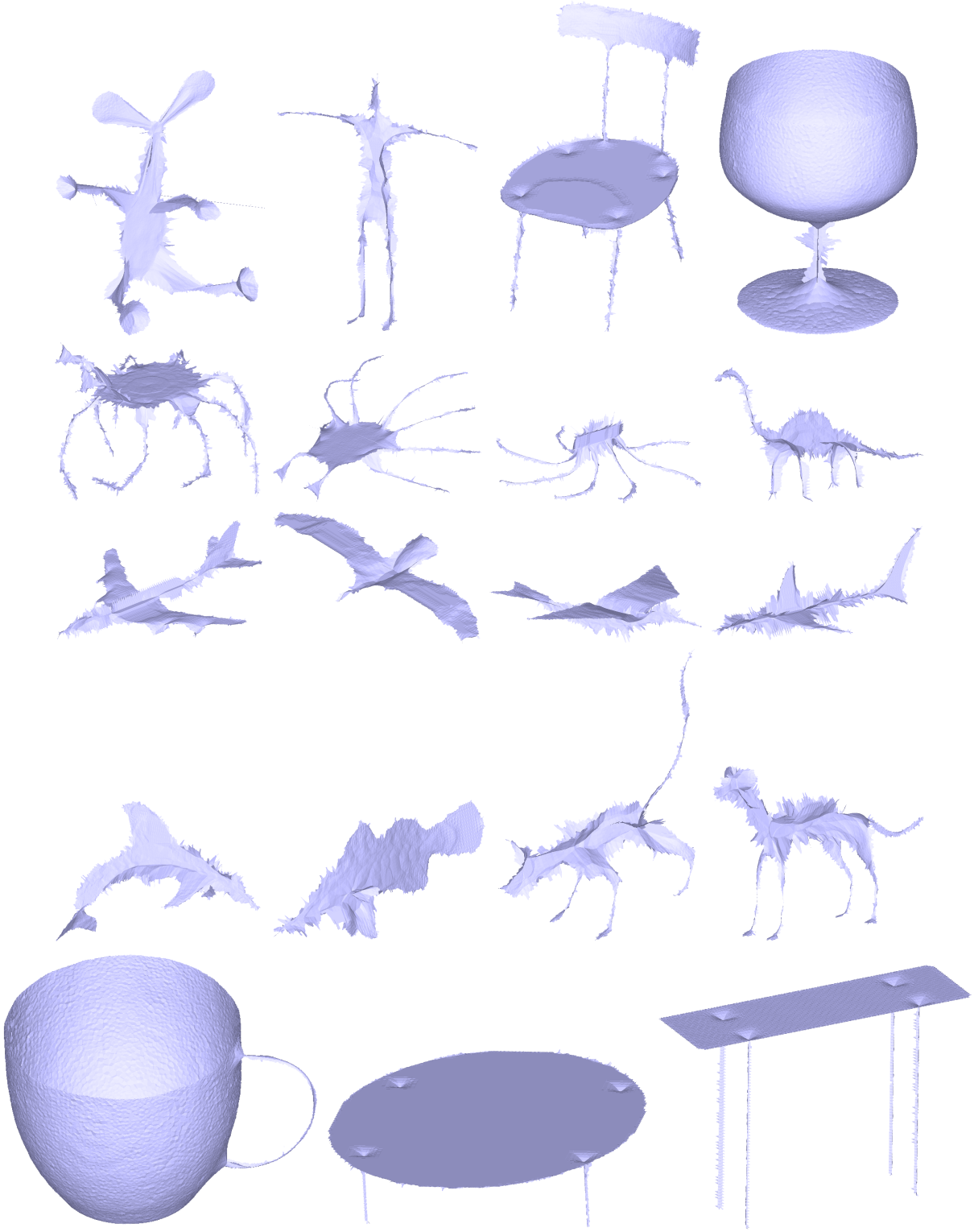

Figure 19: Some skeletons computed by our method ($\varepsilon = 0.01$).